ADVANCED SENSOR RESEARCH Open Access
www.advsensorres.com

Nanoporous Dna Field Effect Transistor with Potential for Random-Access Memory Applications: A Selectivity Performance Evaluation

Volkan Kilinc, Ryoma Hayakawa, Yusuke Yamauchi, Yutaka Wakayama, and Jonathan P. Hill**

Methods to encode digital data items as strands of synthetic DNA followed by selective data retrieval have been demonstrated. However, these initially bio-oriented processes remain slow and not optimized. DNA field-effect transistor (DNA-FET) is studied here as a possible random-access memory (RAM) device for simple, selective and rapid ssDNA fragment retrieval used as data pool identifier. The DNA-FET is based on a co-planar Au-gated fully organic transistor appended with short single-stranded DNA (ssDNA) probes bearing a blocking molecule to prevent partial hybridization and achieve near perfect selectivity for short length ssDNA (up to 45 nt). Examination of transconductance of the novel active layer incorporating a DNA nanopore architecture reveals enhanced binding site accessibility. This, in turn, facilitates discriminatory hybridization, particularly in the physical retrieval of short-length ssDNA from a competitive, concentrated ssDNA background pool consisting of nine different sequences, with at least one nucleotide difference. The DNA-FET exhibits rapid operation (9 min) in the millivolt range, low detection limit (sub-femtomolar), high selectivity and reusability. Considering the straightforward concept, near error-free identification capacity and hypothetically outstanding scalability, the DNA-FET described here has potential as a foundation for further exploration of advanced RAM technology in the DNA data storage process.

1. Introduction

The International Data Corporation has estimated that worldwide by 2025 the quantity of data stored electronically will reach a volume of over 175 zettabytes[1] (in 2007, the value was only 0.29 zettabytes[2]). With the rapid introduction of new data-intensive technologies including the Internet of Things, artificial intelligence, blockchains and metaverses, even more data is expected to be generated so that data storage (volume and rates) might become a limiting factor in the application of those technologies. Furthermore, data must be stored to optimize its security and accessibility, which will also be increasingly challenging with exponential increases in data volumes. Current data storage devices are based on disk and solid-state drives of limited durability (30 years) and data storage capacity whose development is not keeping pace with current or future data growth rate requirements. Therefore, radically new storage media having high data density and durability characteristics should be sought.

Natural systems use deoxyribonucleic acids to store vast amounts of information, and it is an important paradigm of data storage based on several critical advantages. It has an extremely dense data storage capacity,[3] is chemically stable over several centuries under relatively harsh conditions, no power source is required to maintain data,[4] and it is abundant. Researchers have already successfully established the potential of DNA as a storage medium by storing digital data

V. Kilinc, R. Hayakawa, Y. Yamauchi, Y. Wakayama, J. P. Hill
Research Center for Materials Nanoarchitectonics (WPI-MANA)
National Institute for Materials Science (NIMS)
Namiki 1-1, Tsukuba, Ibaraki 305-0044, Japan
E-mail: kilinc.volkanyunus@nims.go.jp; jonathan.hill@nims.go.jp

The ORCID identification number(s) for the author(s) of this article can be found under https://doi.org/10.1002/adsr.202300176

DOI: 10.1002/adsr.202300176

Y. Yamauchi
Australian Institute for Bioengineering and Nanotechnology (AIBN)
The University of Queensland
Brisbane, QLD 4072, Australia

Y. Yamauchi
Department of Materials Process Engineering, Graduate School of Engineering, Nagoya University, Furo-cho, Chikusa-ku
Nagoya University
Nagoya, Aichi 464–8603, Japan

including text, images, music, classified information, etc.[5–8] The application of DNA for data storage is based on five steps: (1) data encoding (convert binary data to A, T, C, G data), (2) synthesis and storage of the corresponding DNA sequence, (3) random access of the data by retrieving the corresponding sequence in a pool of DNA, (4) sequencing of the retrieved DNA and (5) data decoding (A, T, C, G data to binary data). To enable DNA data storage technologies for archiving or for day-to-day uses, and to reduce its cost,[9] progress is required at all of these five steps. For example, for Step (2), enzymatically-driven DNA synthesis is a very promising method offering high coupling efficiency with better reliability and rates than traditional phosphoramidite-based techniques.[10–12] Several new companies have already been established working to improve DNA synthesis yield.[13] Also, as an example of what might be achieved using DNA sequencing, it is now possible to sequence an entire human genome in a single day for only $1000.[14–16] For reference, in 2003 it took thirteen years and almost three billion dollars to complete the Human Genome Project.[15] Such progress has been made possible using high-throughput sequencing by Illumina[17] and nanopore sequencing from Oxford Nanopore Technologies.[18–20] Processing methods with concurrent synthesis and sequencing of DNA[21] are also promising despite their increased complexity.

One of the critical steps in the use of DNA as an efficient data storage medium involves random access of the data. In fact, the physical retrieval of a requested data item contained in a specific DNA sequence from a DNA pool is required to be rapid and error-free. DNA "files" are retrieved conventionally using polymerase chain reaction (PCR):[21] the selected file to be read-out from the pool possesses a sequence that binds to a particular designed primer. When the primer is added, amplification of the target sequence occurs but the sub-pool is then useless for further operations due to the resulting overloading.[22] Non-target DNA sequences can also cross-talk or interfere with the primer leading to retrieval of unwanted files, therefore compromising the data. To overcome these issues, certain modifications have been made based largely on chemical modification of the primers (for instance, by appending magnetic beads) leading to selective physical extraction of the desired information from the DNA pool without compromising the original database.[23,24] A direct random-access approach not involving PCR amplification has also been developed. Initial encapsulation of DNA sub-pools in silica particles labelled with short ssDNA at their surfaces is followed by their sorting by using fluorescent ssDNA probes.[25]

To enable the massive up-scaling of addresses contained in DNA, a PCR-free method is required.[26] DNA-FET technology is an interesting alternative technology for the purpose of random-access memory. By using this technique, base-pairing interactions between complementary sequences near the surface can be measured and transduced according to generation of electrical signals. Nevertheless, this technology faces limitations when dealing with longer DNA lengths and appears unconventional for direct data access, given that data are encoded and stored within a pool of long double-stranded DNA (dsDNA). In fact, the hybridization event, which is only observable with ssDNA pairing, can be screened by charges near the surface (Debye screening effect[27]) resulting in reduced sensitivity and increased error-rates of the device. To overcome this limitation and make DNA-FET suitable as RAM, a potential approach involves considering short ssDNA as a signature component for a designed data pool. Consequently, the identification of a specific ssDNA in a competitive and concentrated medium to mimic large dataset DNA pool would then enable the identification of the corresponding data pool.

In recent research advances based on DNA-FET, the detection of free-DNA in biological samples for cancer diagnosis has been established. It promises performance far superior to the existing sensing techniques with sensitivity to attomolar level[28–31] and high scalability with particular Complementary Metal Oxide Semiconductor (CMOS)-based FET[32] regardless of the selectivity parameter of the device, which is not crucial in this application. However, for DNA-RAM applications, the selectivity parameter of DNA-FET is critical for operation to enable low error rates. While recent advances have been made in improving the selectivity of DNA-FETs,[33–37] none of them provide high selectivity under competitive conditions in concentrated solution. A DNA-FET capable of identifying a diverse DNA sequence with high selectivity and sensitivity in a complex background pool containing different DNA sequences (to reduce error-rate and measurements repeatability), with fast operation, reusability with the same data-set and simple scale-up is therefore required to overcome the intricate retrieval step of the DNA data storage process.

Here we propose an approach based on DNA-FET for near error-free detection of short ssDNA used as a data pool signature component in a concentrated competitive DNA pool. The DNA-FET is based on a poly(3-hexyl) thiophene (P3HT) semiconducting layer and co-planar to the channel area Au-gate electrode tuned with short ssDNA (23-45 nt) probes bearing a blocking molecule to avoid partial hybridization. We show here that this conformational ssDNA active layer allows access to the targeted ssDNA sequence in a highly concentrated pool of nine competitive ssDNA sequences with high discrimination (down to one nucleotide difference), rapid operation (9 min), and reusability with the same data-set. Various sequences of ssDNA probe were tested and the results indicate high scalability potential conditioned by combining several DNA-FETs. Topographic analysis by scanning electron microscope (SEM) reveals nanoporous structures which affect the selectivity of the DNA-FET. Analysis of transconductance based on transistor characteristics and surface plasmon resonance measurements confirm the benefit of the presence of the blocking molecule appended at the ssDNA probe for the higher binding site accessibility discrimination in the physical retrieval of short length ssDNA in a competitive pool. The promising initial findings indicate the potential for utilization of DNA-FET in the random-access stage of the DNA data storage process (**Figure 1**).

2. Experimental Section

2.1. Materials

Solvents and other materials were obtained from Tokyo Kasei Chemical Co. Ltd, Sigma-Aldrich Chemical Co. Ltd, Fujifilm-Wako Chemical Co. Ltd., or Nacalai Tesque Chemical Co. Ltd. And were used as received. Field-effect transistors (FET) with coplanar gate and interdigitated gold electrodes with 30 μm band/gap dimensions were obtained from Metrohm DropSens.

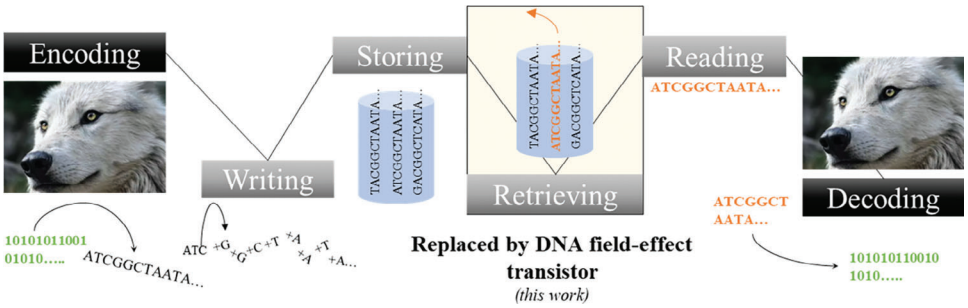

Figure 1. Concept of DNA-FET for data retrieval. Process for the use of DNA as a data storage medium. First, data to be stored is encoded in nucleic data, then it is synthesized and stored in DNA data pool containing multiple nucleotide sequences. Corresponding DNA sequence to be accessed from the pool is retrieved and sequenced followed by a data decoding step (A, T, C, G data to binary data). In this work, DNA-FET is proposed to be used at the step of retrieving short ssDNA as signature component of DNA data pool.

ssDNA were all purchased from IDT (see Table S1 and Table S2, Supporting Information for details).

2.2. Semiconducting Layer Formation

Regioregular P3HT (M_w = 27000–45000) was dissolved in 1,2-dichlorobenzene at concentration 1 mg mL^{-1} and deposited by spin-coating (1 µL, 600 rpm for 10 s then 2000 rpm for 50 s) on the drain-source channel area of the interdigitated electrodes. After annealing at 80 °C for 15 minutes, sulfuric acid (3 µL, 50% w/v) was deposited on the drain-source channel area and left to stand for 10 minutes. The FET was then carefully rinsed with deionized (DI) water and dried at 80°C for 30 minutes. P3HT (1 µL, c = 6 mg mL^{-1} in 1,2-dichlorobenzene) was deposited on the channel area using the same conditions with subsequent annealing under vacuum at 80 °C for 1 h.

2.3. ssDNA Selective Layer Formation

Typically, prior to deposition, ssDNA was diluted in PBS X-0,01 (100 µL) and mixed with dithiothreitol (100 µL at 20 µM) at 45 °C for 10 minutes to cleave dithiol bonds. The solution was then purified by passing through a NAP-10 column (Cytiva). ssDNA probe solution (30 µL, 1.33 µM) was dropped onto the gate electrode of the FET followed by incubation at 25 °C for 24 h. The FET was rinsed with DI water then incubated in DI water at 80 °C for 2 h to remove any impurities.

2.4. Detection Measurements

Competing ssDNA data units (up to eight) were mixed in a pool solution at a total concentration of 10^{-5} M in PBS X-0,01. Another pool solution containing target ssDNA spiked at concentration 10^{-5} M with competing ssDNA data units (up to eight) also being prepared (see Tables S1,S2, Supporting Information for details about the DNA sequences). The P3HT-semiconducting layer-modified-FET was placed in a custom built polychlorotrifluoroethylene (PCTFE) well and PBS X-0,01 (60 µL) was added, covering both the sensing and transducer part of the device. After 10 minutes, five cycles (4 minutes each) of I_D/V_G measurements (Keysight B2912B) were undertaken at V_G = 0.6 V or 0.2 V to −0.6 V with V_D = −0.5 V. After rinsing with DI water, competing ssDNA solution (60 µL) was added at the same point. After 10 minutes, the gate electrode was rinsed with DI water and PBS X-0,01 was added and the I_D/V_G measurements were repeated at least three times. The identical procedure was also repeated for the target DNA spiked competing ssDNA solution.

2.5. Imaging

2.5.1. SEM Imaging

Surface morphology of obtained ssDNA structure was investigated by scanning electron microscopy (SEM S-4800 Hitachi Co.Ltd) operated at 5–10 kV.

2.5.2. AFM Imaging

AFM (SPI-4000, Hitachi High Technologies) with supersharp tip (SSS-NCHR from NanoSensors) was used in tapping mode (T = 3.8 µm, W = 28 µm, L = 125 µm, C = 29 N/m, f = 283 kHz).

2.6. Capacitance Measurements

Transistor tester LCR-TC1 was used to measure the capacitance at the interfaces between the ssDNA functionalized gate electrode/electrolyte and the semiconducting channel/electrolyte.

2.7. SPR Measurements

NanoSPR9 surface plasmon resonance spectrometer (NanoSPR LLC, Milwaukee, USA) with two microchannels was used in pulse mode. Gold-coated substrates provided by the same company were washed with ethanol and DI water prior to the ssDNA selective layer formation protocol. Equation 1 was used to extract reflectivity difference ΔR from the raw data. R was the measured reflectivity, R_0 was the reflectivity of the ssDNA layer without analyte, R_{eq} was the reflectivity of the ssDNA layer at equilibrium with the analyte.

$$\Delta R = \left(1 - \frac{R - R_{eq}}{R_0 - R_{eq}}\right) * 100 \quad (1)$$

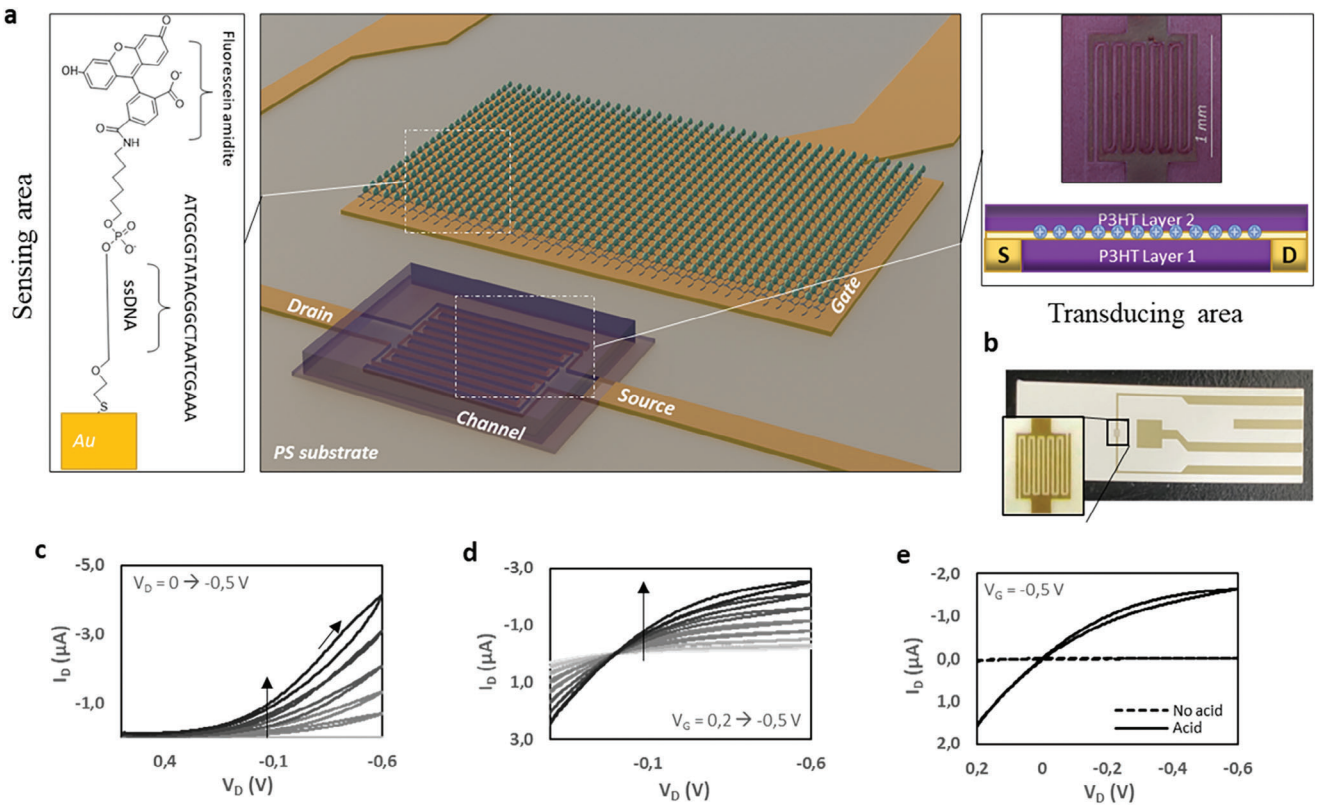

Figure 2. Structure and characterization of the DNA-FET. a) Structure of DNA-FET. Interdigitated gold source-drain electrodes of 30 µm band/gap dimension channel are embedded in two intercalated P3HT layers with sulfuric acid at the interlayer, on flexible polystyrene support. Coplanar gate electrode is grafted with ssDNA probe (23 nt) bearing fluorescein amidite capping molecule by thiol-Au bonding. b) Image of the commercially available FET showing the gold gate electrode in coplanar configuration. c) I_D/V_G characterization, with V_D applied from 0 V to –0.5 V, 0,1 V step. d) I_D/V_D characteristic curve with V_G applied from 0.2 V to –0.5 V at 0.1 V intervals. e) Output curve (V_G = –0.5 V) with/without sulfuric acid interlayer addition. The acid treatment is modifying the local organization of the P3HT layer near the interface allowing to skip the step of high annealing at 150 °C.

3. Results and Discussion

3.1. Design of the DNA-FET

The DNA-FET device is composed of two parts: the sensing area comprising active ssDNA probes capable of interacting with the target ssDNA sequence and the transducer area composed of a semiconducting layer responsive to electrical modulation occurring in the sensing area (**Figure** 2a). For the application of DNA-FET in DNA data access processes, it is critical to enhance the selectivity of the active ssDNA layer in the presence of a competitive background. Therefore, a simple easy-to-reproduce procedure for the transducing part is especially required and is introduced in this work. For this purpose, a procedure involving a commercially available FET structure with Au based gate electrode in coplanar configuration (Figure 2b) and well-known semiconducting polymer, P3HT, has been used. P3HT is an organic p-type semiconducting polymer whose hole mobility (0.1 cm^2 V s^{-1}) is strongly affected by its molecular organization, especially the relative conformations of 3-hexylthiophene units.[38] Optimum hole mobility is usually achieved by applying an annealing step at 150 °C,[39] which promotes organization in films due to a preference for non-coplanarity of 3HT units. However, in this work, high temperature annealing of the FET was not possible since a polystyrene-based material is used as a substrate necessitating an annealing temperature limit of 80 °C to avoid destruction of the devices. To ameliorate for the loss in the semiconducting layer performance, a sulfuric acid layer deposited at the interface of two P3HT layers has been applied (Figure 2e). This technique promotes the local reorganization of 3HT units in the P3HT layer[40] circumventing the necessity of the high temperature annealing process. AFM topographic images indicate a rough (R_a = 20,4 nm) "patchwork" top P3HT layer of around 40 nm thickness (see Figure S2e,f, Supporting Information). Transfer and output curves obtained by transistor measurements (Figure 2c,d.) show typical behavior for p-type FET. The optimized FET (see Figure S1, Supporting Information) exhibits reproducible performance up to 40 measurement cycles with low leakage currents (see Figure S2a,b, Supporting Information), acceptable hysteresis, and works at low voltage resulting in low power consumption. While the performance of the designed FET may not be exceptional, its simplicity makes it well-suited for a comparative study within the scope of this work

For efficient and error-free ssDNA data unit retrieval by DNA-FET, selective detection in a competitive background by active ssDNA probes is required. In conventional ssDNA probe layer implemented in FET, partial hybridization with interfering target ssDNA sequences can affect the transduced electrical signal

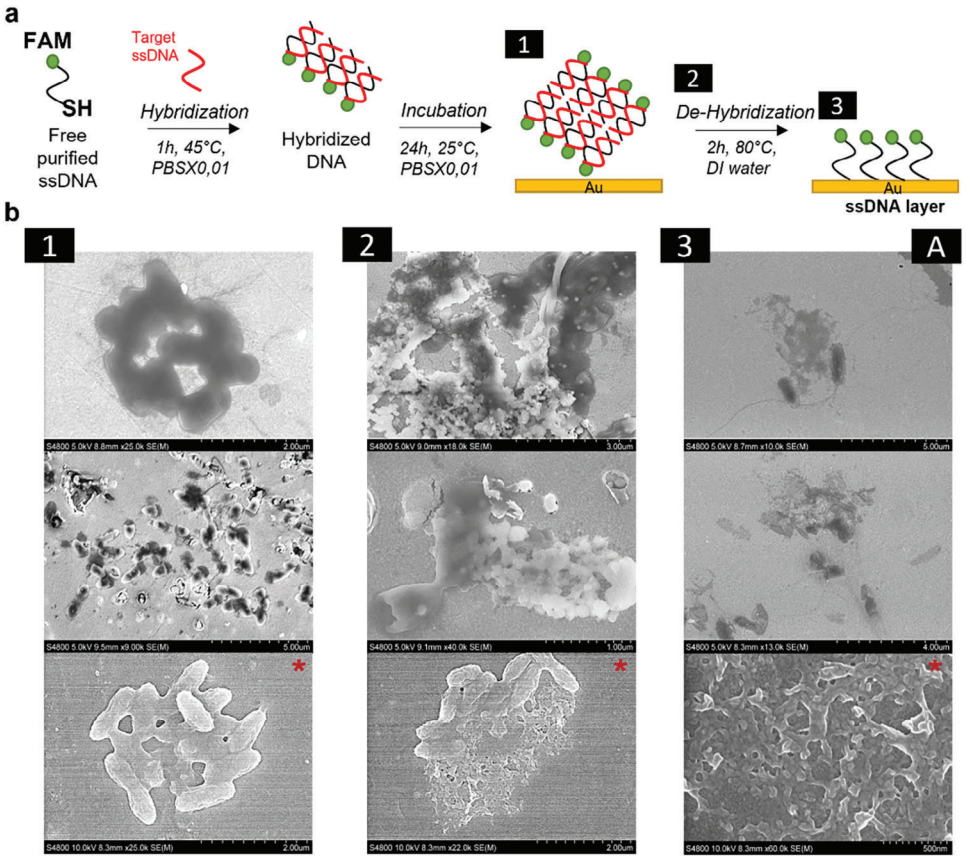

Figure 3. ssDNA layers functionalization: Nanopore-DNA-F method. a) Purified ssDNA probe with FAM capping headgroup and thiol end group was hybridized with its complementary DNA sequence prior to incubation on the Au gate electrode of the FET, followed by a step of de-hybridization to obtain ssDNA layer. b) SEM images illustrating different stages of the functionalization process. In Step 1, capsule-like structures of dsDNA can be observed. In Step 2, capsules are broken and a porous structure with layers is found in Step 3. Images with a red star in the corner are obtained after platinum coating of the samples.

leading to increased error-rates and read-out times of the target data unit. Indeed, the accessibility of the probe to the target molecule is restricted by the physical constraints imposed by the substrate. To eliminate this partial hybridization issue, the introduction of a bulky molecule such as fluorescein amidite (FAM) as a capping headgroup is proposed. Our hypothesis was first tested in solution, where accessibility to the binding site of the probe is ideal. Fluorescence emission by the fluorescein headgroup is quenched only when hybridization occurs with the exactly complementary ssDNA (see Figure S3a, Supporting Information). Perfect selectivity can be therefore attained by appending the FAM headgroup to the ssDNA target to suppress partial hybridization involving complementary nucleotides. However, high concentrations, extended time periods and high purity reagents are required to avoid interference when making observations by using fluorescence spectroscopy.

To avoid these limitations, a new functionalization method is proposed here (**Figure** 3a) (called Nanopore-DNA-F method). The FET Au gate electrode is first functionalized with dsDNA probes appended with the FAM headgroup by thiol-Au grafting reaction. The complementary DNA sequence is then removed by heating the active layer in de-ionized water to obtain the ssDNA functionalized DNA-FET. ssDNA probes used in this study are reported in Table S1 (Supporting Information). This strategy is assumed to improve binding configuration by pre-orienting the ssDNA probe by positioning it at distance more favorable for strong multivalent binding effect than would be free ssDNA probe.[41,42] It should be noted that FAM was chosen here for its pH sensitivity rather than its fluorescence and it is also believed inhibit partial hybridization based on steric hindrance. FAM can also aggregate by protonation of its acid carboxyl group at pH around 7[43] (see Figure S3b, Supporting Information). SEM images (Figure 3b) show the variations in structure observed during the functionalization process. Capsule-like structures of around 200 nm height present initially are broken by heating leading to a nanoporous structure and layers. Nanoporous structures are unique to this functionalization method as showed in the comparative study (see Figure S4, Supporting Information) and confirmed by optical microscopy observations (see Figure S5, Supporting Information). Furthermore, ssDNA particle size and nanopore dimension appear to be dependent on the ssDNA probe lengths (see Figure S6, Supporting Information). For ssDNA probe with 23 nt, nanopores are measured to be 28 nm +/-5 nm (see Figure S7, Supporting Information). The combination of the FAM capping molecule with the prehybridization step in the Nanopore-DNA-F leads to a nanoporous ssDNA structure at the gate electrode. It is important

to emphasize that the functionalization of the gate electrode does not notably reduce the channel conductivity in the FET due to the partial coverage of the gate surface (see Figure S2d, Supporting Information).

3.2. Selectivity of The ssDNA Active Layer

$$I_D = \frac{W}{2L}\mu C_{TOT}\left(V_G - V_{th}\right)^2 \quad (2)$$

Equation 2 defines operation of the FET in the saturation regime,[44] where I_D is the current in the channel of the semiconducting layer, $\frac{W}{2L}$ is the dimension of the channel area, μ is the conductivity of the semiconducting layer, C_{TOT} is the sum of the overall capacitance of the device (channel capacitance/insulating layer, insulating layer/electrolyte, gate electrode/electrolyte), V_G is the applied gate voltage, and V_{th} is the threshold voltage. The value of V_{th} in the saturation regime can be correlated with occurrence of the hybridization event involving the target ssDNA near the gate surface. Pairing of the ssDNA leads to chemical doping of the selective layer on the gate electrode, affects its electrochemical potential (ΔE_G), and modulates the work function.[45,46] This in turn tunes the operating voltage range of the FET without perturbing the transport properties and stability of the channel material. The coplanar gate electrode structure is therefore crucial to achieve segregated sensing operations without polluting the semiconducting layer to avoid interference which might modify the channel transport properties. Moreover, as a precaution, the maximum gate voltage was set at –0.6 V to avoid leakage current (see Figure S2c, Supporting Information) and maintain specific DNA conformation (higher electric fields can affect the DNA conformation[46]).

Selectivity performance of the nanoporous ssDNA layer obtained by the Nanopore-DNA-F was evaluated by using Equation 3

$$S = \left(1 - \frac{V_{th\,1} - V_{th\,0}}{V_{th\,2} - V_{th\,0}}\right) * 100 \quad (3)$$

where S is the selectivity ratio, $V_{th\,0}$ is extrapolated from the backward I_D/V_G transfer curves with only PBS X-0,01, $V_{th\,1}$ from transfer curves after incubation with competitive ssDNA pool with at least one-nucleotide difference in DNA sequence, and $V_{th\,2}$ from the same pool containing spiked target ssDNA. The closer the selectivity ratio S is to 100%, the better the discrimination of the target ssDNA from the background is. In contrast, if S approaches 0%, differentiation of the target ssDNA from the background is difficult.

Comparison of the selectivity ratio between ssDNA layer obtained by the Nanopore-DNA-F and the conventional method (no FAM, no pre-hybridization step) was made (**Figure 4**). Compared to the conventional method, the results indicate almost perfect discrimination when complementary pairing occurs with the target ssDNA with the newly designed ssDNA layer, even in the competitive ssDNA pool containing one-nucleotide different sequence. Control measurements were undertaken to validate the selectivity ratio determination method (see Figure S8, Supporting Information). To illustrate the importance of the FAM headgroup and pre-hybridization step in the nanostructural organization of the selective ssDNA, S was measured in the absence of the FAM headgroup and without pre-hybridization step (**Figure 5**). The nanoporous structure is obtained only when FAM headgroup is present and the prehybridization step is performed. In the absence of FAM, only non-porous aggregates were obtained. S is higher than 50% only when the nanoporous structure is present, suggesting increased accessibility of the target ssDNA to the binding site on the substrate, possibly induced by the nanostructured form.

The observed high selectivity of the ssDNA active layer was cross-checked by using surface plasmon resonance (SPR) measurements and compared with ssDNA layer obtained without the step of pre-hybridization (B), without the FAM capping group on the ssDNA probe (C), and with the standard functionalization method (D) (no FAM and no pre-hybridization) (see Figure S9, Supporting Information). Saturation of the probes occurs after 30 minutes. Without FAM capping-molecule and pre-hybridization step of the probes (layer B, C, & D), reflectivity evolves similarly regardless of whether the target DNA is spiked in the competitive DNA pool or not. Discrimination is therefore not possible, as observed by transistor measurements. For the ssDNA active layer obtained by using the newly designed functionalization method, competitive ssDNA does not interact at all with the absence of kinetic evolution. A strong discrimination characteristic of ssDNA selective layer is therefore confirmed by transistor measurements and qualitative analysis by SPR measurements.

3.3. Performance and Limitations of DNA-FET for Random Data Access

The performance of the DNA-FET for data access applications involving different ssDNA selective layer configurations and conditions was evaluated by comparing the calculated selectivity ratio S (Equation 3) for the retrieval of target short ssDNA in a competitive pool. The results (**Figure 6a** and see Figure S10a,b,c and Table S2, Supporting Information for the corresponding I_D/V_G transfer curves and ssDNA sequences) indicate that it is possible to achieve high discrimination with different ssDNA sequence probes in a highly concentrated pool containing nine competitive data units (with at least one data unit with one nucleotide difference). Even when the target ssDNA concentration is low (10^{-16} M) (Figure 6b), detection and discrimination of the ssDNA is observed in the competitive pool. The results therefore show the opportunity for high scalability (i.e., for ssDNA probes of 20 nt length, 4^{20} (1 099 511 627 776) DNA sequence combinations are possible). The DNA-FET can also be recycled and reused (Figure 6c) by simply heating the ssDNA modified gate electrode in DI water at 80°C, even if I_D is decreased due to the organic semiconducting layer alteration. In terms of ssDNA identification time, our measurements (Figure 6d) show that it can be reduced to 9 min for one ssDNA read. It is also worth mentioning that parallel ssDNA identification by DNA-FET is technically feasible although it has not been demonstrated here.

Despite the remarkable performance in terms of the promising scalability of DNA-FET, there are also some limitations. Increasing length of the ssDNA probes (35 and 45 nt) decreases the selectivity ratio S (**Figure 7c**), even if it is remains high compared to the standard functionalization method. Nanoporous

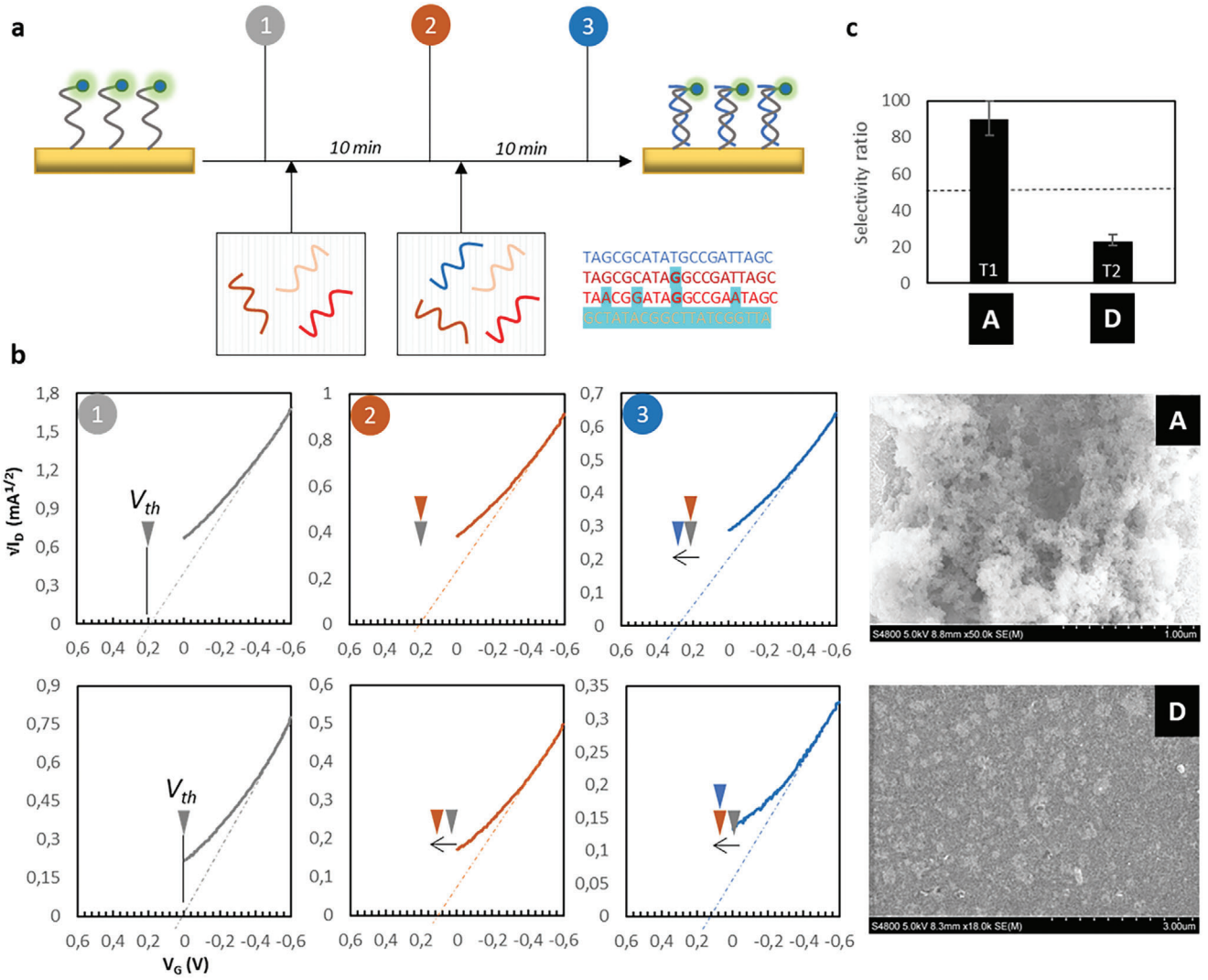

Figure 4. Selectivity of ssDNA layers obtained by the Nanopore-DNA-F method: comparison with the standard method. a) Schematic representation of the selectivity evaluation protocol by transistor measurements. An initial measurement in PBS X-0,01 (grey color) was used as a control reference. Subsequent 10 min incubation with the competitive ssDNA pool (10^{-5} M) containing at least one ssDNA sequence with one nucleotide difference was performed. After vigorous rinsing with deionized water, PBS X-0,01 was added and I_D/V_G measurement was performed (indicated by red). The same step was repeated with competitive ssDNA pool spiked with the target ssDNA (10^{-5} M) (indicated by blue lines). b) I_D/V_G transfer curves of the DNA-FET prepared using the Nanopore-DNA-F method (A) and the standard functionalization method (D) (no FAM and no pre-hybridization). The selective layers are illustrated with the corresponding SEM images. V_D was fixed at –0.5 V. At least three measurement cycles were performed for each step. Grey traces correspond to absence of ssDNA (only PBS), red traces in the presence of competitive ssDNA, blue traces in the presence of competitive ssDNA spiked together with target DNA. c) Selectivity ratio S of the layer A and D calculated by using Equation 2 from the extrapolated threshold voltages V_{th} from the backward I_D/V_G transfer curves at each step. Error bars are the SD of three measurement cycles. Triangles indicate the position of the extrapolated V_{th} for each curve.

dimensions, which depend on the ssDNA probes lengths (see Figure S6, Supporting Information), also affect the selectivity ratio. Another factor influencing the selectivity ratio is the secondary structure folding temperature T_m of the ssDNA probes. Below the T_m, ssDNA forms secondary structures by homo-hybridization (i.e., donut structures). For ssDNA probes with T_m closer to room temperature, reduced selectivity is observed (Figure 7b). Here we propose that T_m is a critical parameter in the formation of the nanoporous structure, which impacts the selectivity ratio. By fine-tuning the incubation temperature for each ssDNA probe, we believe that this limitation can be overcome. Additionally, further studies are required to explore the impact of the nucleotide sequence composition, which is directly correlated to T_m, on the formation of nanoporous structures. Regarding the persistence of the nanoporous structure, although this has not been fully investigated here, samples of the structure stored for one year exhibit similar binding efficiencies of ssDNA probes as the freshly prepared devices.

Integration of the DNA-FET in the current DNA storage process as direct random-access solution of the data stored in

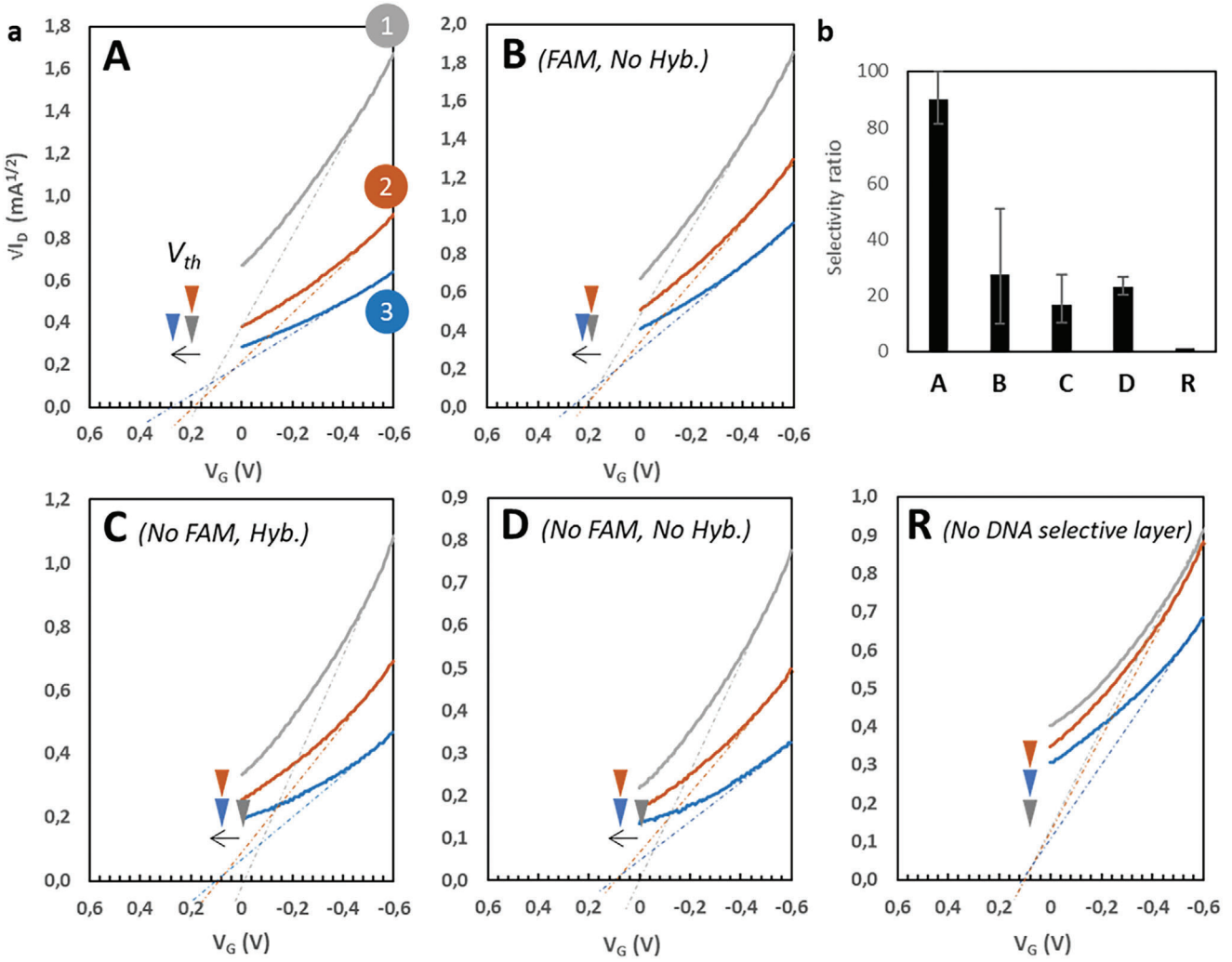

Figure 5. Selectivity comparison of the Nanopore-DNA-F method when ssDNA probe is modified a) I_D/V_G backward transfer curves of the DNA-FET prepared using the Nanopore- DNA-F method (A), using the Nanopore-DNA-F method but without the prehybridization step (B), using the Nanopore-DNA-F method but without the FAM capping group on the ssDNA probe (C), using the conventional functionalization method (D) (no FAM and no pre-hybridization), and without the ssDNA selective layer (R). V_D was fixed at −0.5 V. At least three measurement cycles were performed for each step. Grey traces correspond to absence of ssDNA (only PBS), red traces are in the presence of competitive ssDNA, blue traces are in the presence of competitive ssDNA spiked together with target DNA. b) Selectivity ratio *S* of the layer A, B, C, D, and R calculated by using equation 2 from the extrapolated threshold voltages V_{th} obtained on the backward I_D/V_G transfer curves at each step. Error bars are the SD of three measurement cycles. Triangles indicate the position of the extrapolated V_{th} for each curve.

dsDNA (by considering maximum length of 45 nt) has also been considered. For this purpose, DNA-FET is required first to be prepared using dsDNA data units. Subsequent unpairing of ds-DNA by heating at 100°C is performed prior to transistor measurements. The results indicate reduced selectivity (Figure 7a) for this unoptimized process caused by rapid rehybridization of the ssDNA. Also, captured ssDNA data units need to be released from the surface and introduced to a sequencing device for integration as a random-access tool in a data storage process. As the concentration of released ssDNA is lower than the required minimum concentration for sequencing, some technical adjustment is required (i.e., increasing ssDNA probe density) prior to implementation of this technique as direct random-access of DNA data unit in the current data storage process.

3.4. Proposed Sensing Mechanism of DNA-FET

In order to determine the limit of detection and sensitivity of the DNA-FET, the gate electrode coated with the ssDNA selective layer was incubated with solutions containing different concentrations of target ssDNA. A linear response of the DNA-FET was obtained in the range 10^{-19} M – 10^{-11} M with a sensitivity of 10 mV dec^{-1} (**Figure** 8a,b). These low limits and wide ranges can be explained by two phenomena: first, transient electric field applied by the gate electrode in the measurement environment can tilt the ssDNA probes, resulting in longer Debye lengths.[27,47] Furthermore, the use of dilute PBS enables lower ionic strength and subsequently larger Debye length. Second, the very thin insulating electric double layer at the P3HT/electrolyte interface

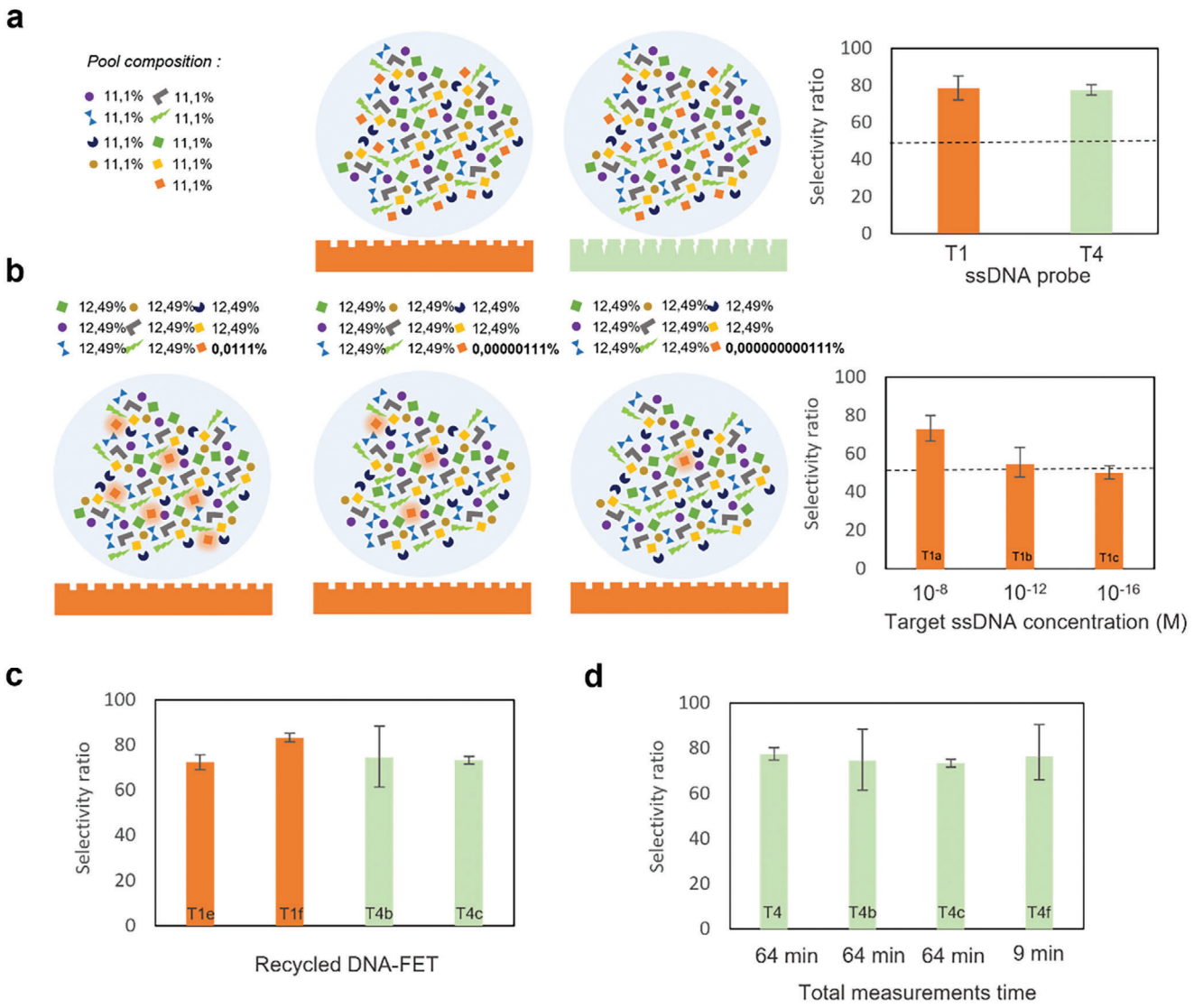

Figure 6. Selectivity performance of the DNA-FET for ssDNA retrieval. a) Selectivity ratio *S* measured with two different ssDNA probe sequence of 23 nt in a pool composed of 9 different ssDNA sequences with at least one having one-nucleotide difference from the probe sequence. The concentration of the pool was fixed at 10 µM. b) Selectivity ratio *S* measured with the ssDNA probe sequence (T1) in a pool composed of nine different ssDNA sequences with at least one with one-nucleotide difference from the probe. The concentration of the pool background was fixed at 10 µM with a digressive concentration of the target ssDNA sequence. c) Selectivity ratio *S* measured with two different ssDNA probes (T1 & T4) and four DNA-FET in a pool of nine competitive ssDNA sequences after a step of device recycling based on heating the active layer in DI water at 80 °C for 2 h. d) Selectivity ratio *S* comparison with faster measurement time. The measurement time for the sample T4f was decreased by removing the incubation steps and decreasing the I_D/V_G transfer curve recording time (from 4 min to 1 min for each cycle). Error bars correspond to the SD of three measurements.

contributes to the high sensitivity as the capacitance is inversely proportional to the thickness of the insulating layer. The combination of these phenomena might account for the attained ultralow detection limit. Decreases were also observed for I_D and the transconductance, g_m (Figure 8c). Transconductance corresponds to the expression μC_{TOT},[48] the slope of the linear region of the transfer curve. Values obtained on initial observation might reasonably be assigned to a bias stress effect.[49] However, subsequent observations indicate that is not the case. In fact, V_{th} did not vary during repeated measurements at the same concentration (by adding fresh solution), and only resulted in reductions in I_D and g_m (see Figure S11a,b, Supporting Information.)

To explain the sensing mechanism, we hypothesize that a decrease in the value of the transconductance g_m is associated only with a decrease of the capacitance of the gate electrode/electrolyte interface C_s. In fact, capacitance drop at the ssDNA functionalized gate electrode and electrolyte interface is observed in the presence of target ssDNA (see Figure 11Sc, Supporting Information). It is unlikely that interference which might alter channel transport properties will occur since we have performed segregated sensing operations without contaminating the semiconducting layer. Decrease of C_s occurs after grafting of the ssDNA probe, hybridization of the ssDNA probe with the target ssDNA, and when the sensing area is overloaded by aggregated DNA.

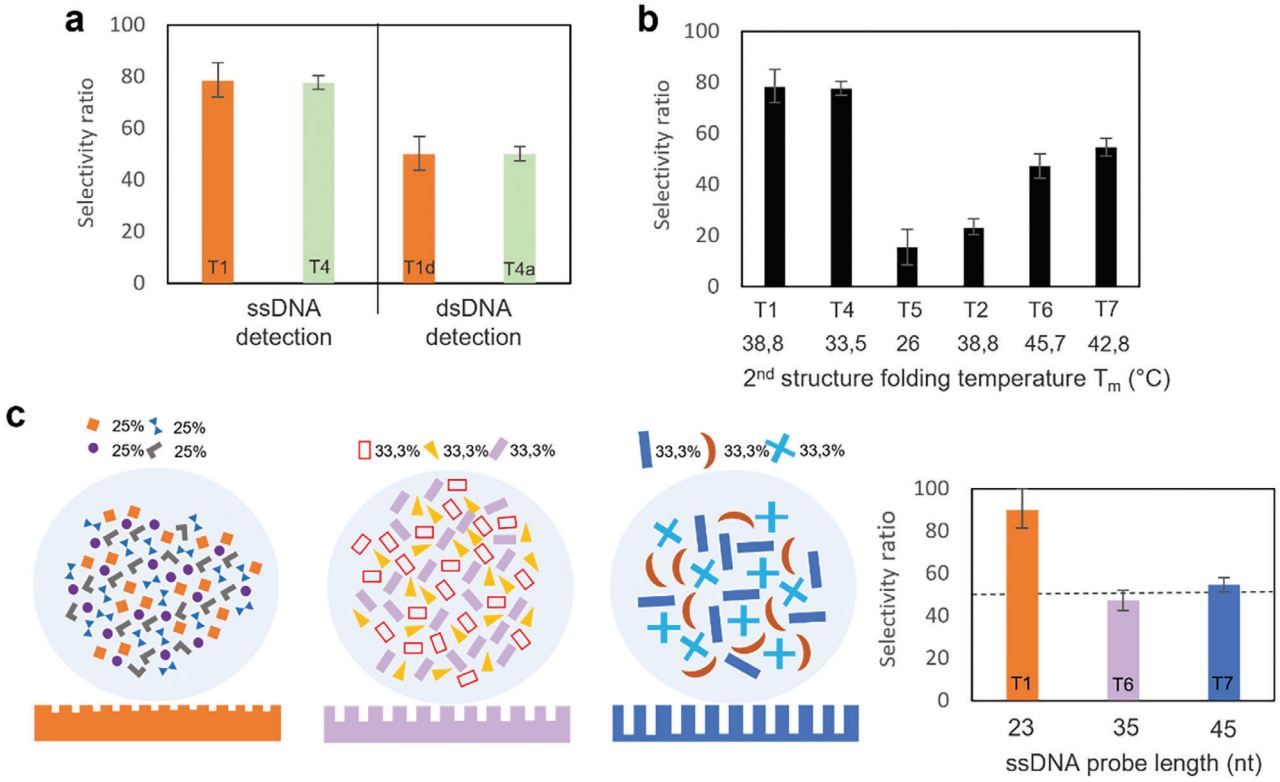

Figure 7. Characteristics and performance limitations of the DNA-FET. a) Selectivity ratio *S* comparison for identification of ssDNA directly or ssDNA obtained after heating dsDNA solution at 100 °C for 20 min. Two different ssDNA probes were used (T1 & T4). b) Selectivity ratio *S* comparison with the second structure folding temperature T_m for different ssDNA probes used in the experiments. c) Selectivity ratio *S* measured with three different ssDNA probe sequences of 23, 35, 45 nt length respectively in a pool composed of at least three different ssDNA sequences where at least one sequence has a one-nucleotide difference from the probe. The concentration of the pool background was fixed at 10 µM. The error bars correspond to SD of three measurements.

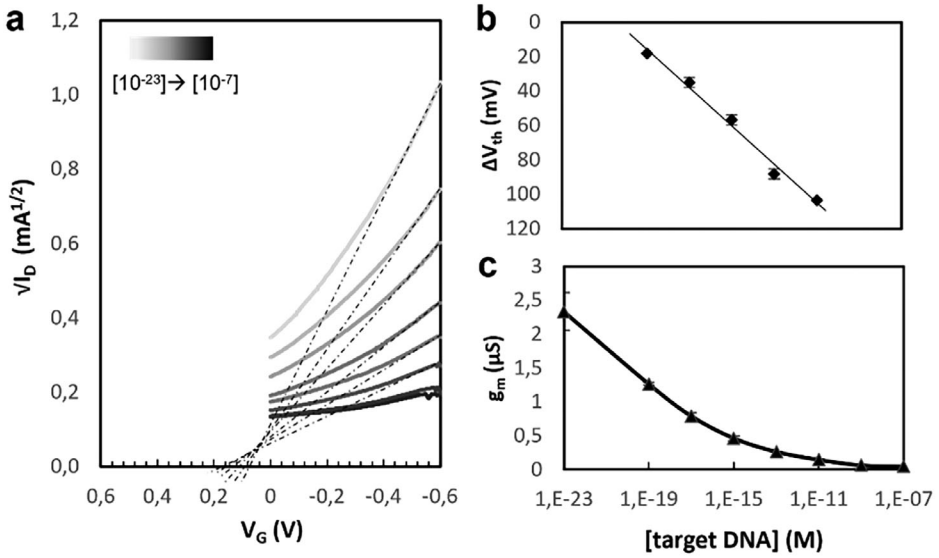

Figure 8. Detection range of the DNA-FET and transconductance evolution. a) Backward transfer curves of DNA-FET functionalized with the new method and incubated for 10 minutes with solutions having increasing concentrations of target ssDNA, from 0 (10^{-23} M) to 10^{-7} M, and measured in PBS X-0,01 after washing with DI water. Three cycles were performed before recording. V_D was fixed at −0.5 V. b) Calibration curve of V_{th} obtained from the transfer curves normalized against the point at 0 [10^{-23} M]. Reported standard deviation are for N = 3 measurements. It was not possible to determine the V_{th} for concentrations under 10^{-11} M because of the low I_D. c) Transconductance g_m obtained from the slope of transfer curves. Reported standard deviation are for N = 3 measurements.

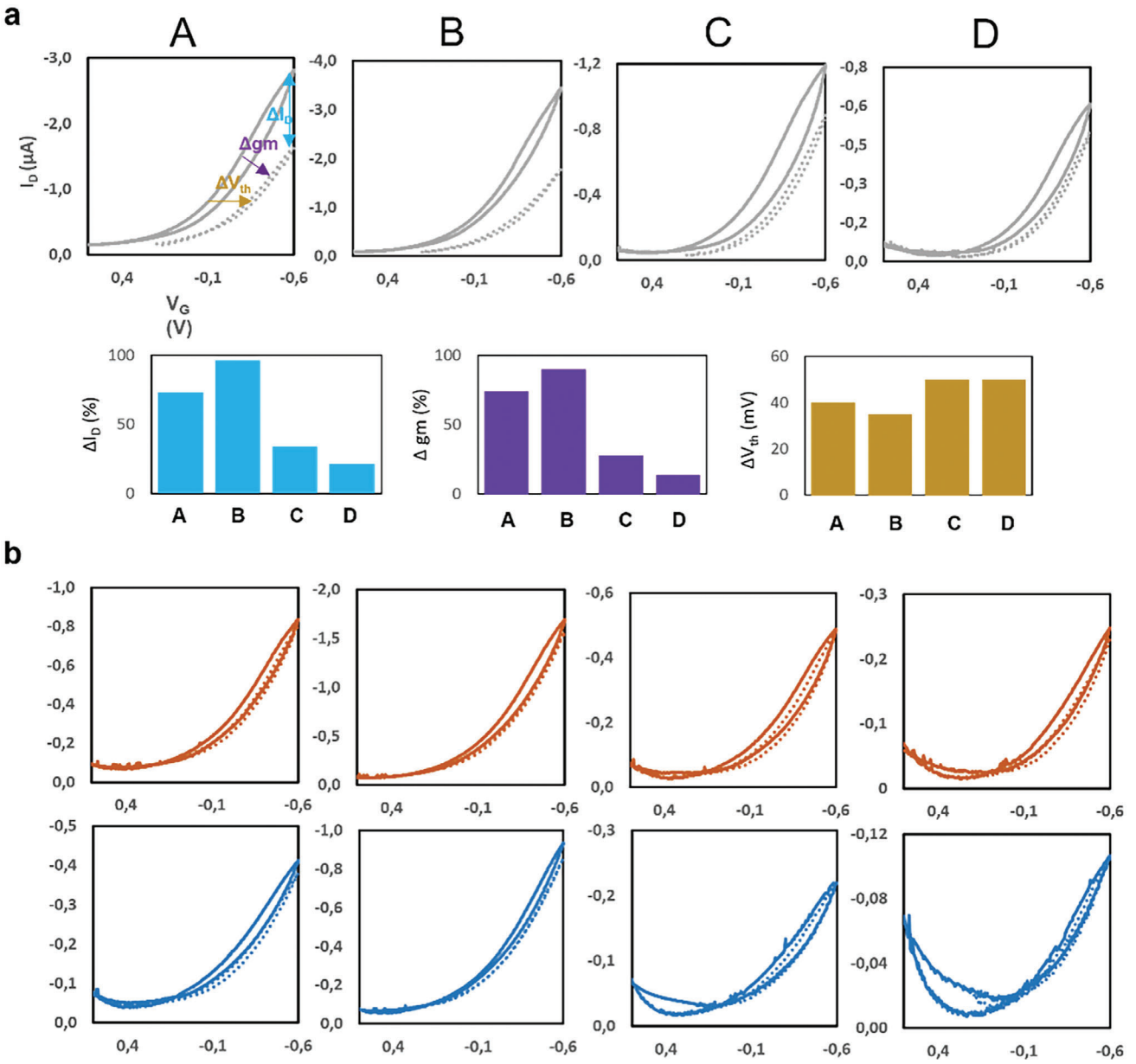

Figure 9. Transfer curves obtained at high and low off-state gate voltages. a) DNA-FET transfer curves with ssDNA functionalized by Nanopore-DNA-F method (A) and modified Nanopore-DNA-F method (B, C, D, see Figure S4, Supporting Information) during PBS X-0,01 measurement cycles at a high off-state gate voltage (when it starts at 0.6 V, full-line) and low off-state gate voltage (when it starts at 0.2 V, dashed-line). Five cycles were performed prior to data collection. Differences in the channel current ΔI_D at $V_G = -0.6$ V (turquoise color), transconductance Δg_m (purple colour) and ΔV_{th} (gold colour) for measurement cycles at high and low off-state gate voltages were extracted from the backward transfer curves. V_{th} shifts occurred in the direction of the applied gate voltage (negative side). b) Presented selective layers with competitive ssDNA solution (red) or competitive ssDNA solution spiked with target ssDNA (blue) at high concentration (10^{-5} M) at a high off-state voltage (starting at 0.6 V, full-line) and low off-state voltage (starting at 0.2 V, dashed-line). No significant modification is observed between high and low off-state voltage measurements when the selective layer is saturated.

Shift of the V_{th} is observed only when complete hybridization occurs. Aggregation of FAM molecules of the ssDNA probes should be favored by the complete pairing of the nucleotide bases. This also acts as a molecular gate and can lock the access of competitive ssDNA near the surface therefore preventing variation of the working potential of the gate electrode.

To confirm our hypothesis that the transconductance and the channel current are correlated independently of the threshold voltage induced by the concentration changes in the captured target ssDNA (Equation 2), transfer curves obtained by ssDNA selective layers A, B (with FAM) and C, D (without FAM) incubated in DNA-free solution (only PBS X-0,01), competitive ssDNA solution or competitive ssDNA solution spiked with target ssDNA at high concentration (10^{-5} M) were compared with transistor measurement cycles starting at 0.6 V (called high off-state gate voltage) and ending at −0.6 V or starting at 0.2 V (called low

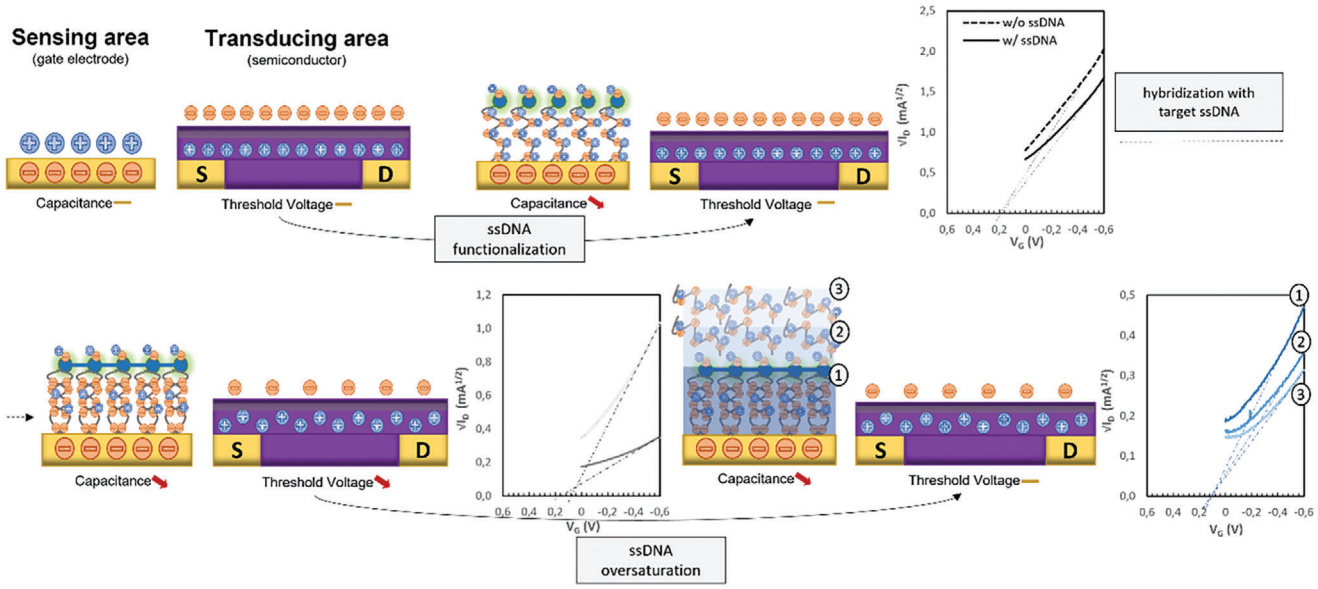

Figure 10. Proposed discriminatory sensing mechanism. Scheme of the proposed sensing mechanism showing the DNA-FET sensing area on the gate electrode at V_G= −0.6 V comprising the ssDNA probes and the transducing area composed of P3HT semiconducting channel at different steps: ssDNA functionalization, hybridization and over-saturation. Relative changes in the capacitance at the gate electrode/electrolyte and the threshold voltage are indicated below each scheme. I_D/V_G transfer curves of each step are indicated next to each scheme.

off-state gate voltage) and ending at −0.6 V. At higher off-state voltage, when binding sites are vacant (i.e., in neat PBS X-0,01), the selective layers containing ssDNA layer with FAM (A, B) are expected to condense near the surface since the FAM moieties are negatively charged at pH 7.4 (i.e., pH +/- 0.2 of the PBS), leading to higher charge density due to ion trapping than at lower off-state voltage (**Figure 9a**). Transfer curves confirm that a high value of ΔI_D (difference of I_D at V_G = −0.6 V for measurement cycles at high and low off-state gate voltage) is observed for the vacant selective layers A, B compared to layers C, D. A similar trend is observed for the transconductance. For V_{th}, a constant shift in the negative side (direction of the applied gate voltage) is observed for all the vacant selective layers, which is typically observed in the case of bias-stress effects.[49] In contrast, when the surface is overloaded with ssDNA (complementary or not) (Figure 9b), ΔI_D and Δg_m are almost unmodified regardless of the off-state voltage, suggesting that DNA surface aggregation impedes DNA conformational changes in the vicinity of the surface. These results highlight that a decrease in I_D is induced by a decrease in the capacitance of the gate electrode/electrolyte interface C_s.

We can therefore confirm our initial hypothesis concerning the sensing mechanism: any unreacted molecules or parasitic reactions are associated with a decrease in capacitance caused by screening of the gate electrode and the consequent weakening of the applied electrical field.[50,51] However, when hybridization occurs near the surface, strong H-bonds formed by paired nucleotides result in modification of the work function of the gate electrode leading to modulation of V_{th}[52] (**Figure 10**). This effect is further enhanced by the aggregation of adjacent FAM molecules in the selective layer[53] which can arise only when complete DNA pairing is achieved. In fact, when the FAM molecules are linked on the phosphate backbone of the ssDNA probe and are sufficiently mutually remote, they can rotate independently of any constraint imposed by the nucleotides.[43,54] Once aggregated, however, they can operate as a molecular gate preventing competitive ssDNA access to areas close to the gate electrode and preventing variations in gate electrode work function.

4. Conclusion

In this work, we demonstrate direct random access of short ssDNA sequence (23, 35 and 45 nt) in a highly concentrated (10^{-5} M) competitive pool (nine unique ssDNA sequence with at least one with one-nucleotide difference) by using an easy-to-prepare DNA-FET structure operating in the millivolt range. Fluorescein amidite FAM has been used effectively as a capping molecule to prevent partial ssDNA hybridization. By applying lower and higher gate voltages in the off state during transistor measurements, we are able to elucidate the mechanism responsible for the high degree of discrimination. It is also apparent from the measurements that nanostructuring of the active layer including well-defined nanopores which promote selectivity, is critical for the device operation to achieve near error-free identification of the DNA pool signature component. It can be operated in a low target ssDNA concentration regime (10^{-16} M) in a concentrated competitive pool (10^{-5} M), reducing the quantities of DNA material required for operation, thus extending the lifetime of random-access operation. Nevertheless, to obtain functionality as an efficient RAM in the DNA data storage process, further critical modifications are imperative. DNA-FETs present advantages in terms of potential scalability. Through the use of the Nanopore-DNA-F method to functionalize multiple combined CMOS-based transistors with various ssDNA probes to simulate parallel operation, a near error-free, fast-operating, reusable, and robust device can be achieved. Subsequently, with the implementation of

capsule-like structures to contain substantial data quantities with short unique ssDNA identifier, we are confident that our ultra-selective and sensitive DNA-FET can serve as a viable technology for retrieving DNA data units stored in an archive or active pool.

Supporting Information

Supporting Information is available from the Wiley Online Library or from the author.

Acknowledgements

This work was supported by funding from Postdoctoral Fellowship of Japan Society for the Promotion of Science program (JSPS P21747). This work was partly supported by World Premier International Research Center Initiative (WPI Initiative), MEXT, Japan. The authors are grateful to the JST-ERATO Yamauchi Materials Space Tectonics Project (JPMJER2003). This work used the Queensland node of the NCRIS-enabled Australian National Fabrication Facility (ANFF).

Conflict of Interest

The authors declare no conflict of interest.

Data Availability Statement

The data that support the findings of this study are available from the corresponding author upon reasonable request.

Keywords

DNA data storage, DNA field-effect transistors, nanoporous DNA layer, random-access memory

Received: November 14, 2023
Revised: January 8, 2024
Published online: February 2, 2024

[1] M. Gu, X. Li, Y. Cao, *Light Sci. Appl.* **2014**, *3*, 2.
[2] M. Hilbert, P. López, *Science* **2011**, *332*, 60.
[3] L. Organick, Y. J. Chen, S. Dumas Ang, R. Lopez, X. Liu, K. Strauss, L. Ceze, *Nat. Commun.* **2020**, *11*, 616.
[4] R. N. Grass, R. Heckel, M. Puddu, D. Paunescu, W. J. Stark, *Angew. Chem. – Int. Ed.* **2015**, *54*, 2552.
[5] N. Goldman, P. Bertone, S. Chen, C. Dessimoz, E. M. Leproust, B. Sipos, E. Birney, *Nature* **2013**, *494*, 77.
[6] L. C. Meiser, B. H. Nguyen, Y. J. Chen, J. Nivala, K. Strauss, L. Ceze, R. N. Grass, *Nat. Commun.* **2022**, *13*, 352.
[7] K. Halvorsen, W. P. Wong, *PLoS One* **2012**, *7*, 9.
[8] A. Doricchi, C. M. Platnich, A. Gimpel, F. Horn, M. Earle, G. Lanzavecchia, A. L. Cortajarena, L. M. Liz-Marzán, N. Liu, R. Heckel, R. N. Grass, R. Krahne, U. F. Keyser, D. Garoli, *ACS Nano* **2022**, *16*, 17552.
[9] L. Ceze, J. Nivala, K. Strauss, *Nat. Rev. Genet.* **2019**, *20*, 456.
[10] M. A. Jensen, R. W. Davis, *Biochemistry* **2018**, *57*, 1821.
[11] S. Palluk, D. H. Arlow, T. De Rond, S. Barthel, J. S. Kang, R. Bector, H. M. Baghdassarian, A. N. Truong, P. W. Kim, A. K. Singh, N. J. Hillson, J. D. Keasling, *Nat. Biotechnol.* **2018**, *36*, 645.
[12] H. H. Lee, R. Kalhor, N. Goela, J. Bolot, G. M. Church, *Nat. Commun.* **2019**, *10*, 2383.
[13] M. Eisenstein, *Nat. Biotechnol.* **2020**, *38*, 1113.
[14] L. Organick, S. D. Ang, Y. J. Chen, R. Lopez, S. Yekhanin, K. Makarychev, M. Z. Racz, G. Kamath, P. Gopalan, B. Nguyen, C. N. Takahashi, S. Newman, H. Y. Parker, C. Rashtchian, K. Stewart, G. Gupta, R. Carlson, J. Mulligan, D. Carmean, G. Seelig, L. Ceze, K. Strauss, *Nat. Biotechnol.* **2018**, *36*, 242.
[15] E. R. Mardis, *Nature* **2011**, *470*, 198.
[16] J. Shendure, S. Balasubramanian, G. M. Church, W. Gilbert, J. Rogers, J. A. Schloss, R. H. Waterston, *Nature* **2017**, *550*, 345.
[17] S. Goodwin, J. D. McPherson, W. R. McCombie, *Nat. Rev. Genet.* **2016**, *17*, 333.
[18] D. Deamer, M. Akeson, D. Branton, *Nat. Biotechnol.* **2016**, *34*, 518.
[19] K. Chen, J. Kong, J. Zhu, N. Ermann, P. Predki, U. F. Keyser, *Nano Lett.* **2019**, *19*, 1210.
[20] S. Chalapati, C. A. Crosbie, D. Limbachiya, N. Pinnamaneni, *Open Res. Eur.* **2021**, *1*, 47.
[21] C. Xu, B. Ma, Z. Gao, X. Dong, C. Zhao, H. Liu, *Sci. Adv.* **2021**, *7*, eabk0100.
[22] Y. J. Chen, C. N. Takahashi, L. Organick, C. Bee, S. D. Ang, P. Weiss, B. Peck, G. Seelig, L. Ceze, K. Strauss, *Nat. Commun.* **2020**, *11*, 3264.
[23] K. J. Tomek, K. Volkel, A. Simpson, A. G. Hass, E. W. Indermaur, J. M. Tuck, A. J. Keung, *ACS Synth. Biol.* **2019**, *8*, 1241.
[24] K. N. Lin, K. Volkel, J. M. Tuck, A. J. Keung, *Nat. Commun.* **2020**, *11*, 2981.
[25] J. L. Banal, T. R. Shepherd, J. Berleant, H. Huang, M. Reyes, C. M. Ackerman, P. C. Blainey, M. Bathe, *Nat. Mater.* **2021**, *20*, 1272.
[26] A. El-Shaikh, M. Welzel, D. Heider, B. Seeger, *NAR Genomics Bioinforma* **2022**, *4*, 1-1.
[27] S. Lai, M. Barbaro, A. Bonfiglio, *Appl. Phys. Lett.* **2015**, *107*, 103301-1.
[28] M. T. Hwang, M. Heiranian, Y. Kim, S. You, J. Leem, A. Taqieddin, V. Faramarzi, Y. Jing, I. Park, A. M. van der Zande, S. Nam, N. R. Aluru, R. Bashir, *Nat. Commun.* **2020**, *11*, 1.
[29] C. F. Chang, M. S. C. Lu, *IEEE Sens. J.* **2020**, *20*, 8930.
[30] Y. Liang, M. Xiao, D. Wu, Y. Lin, L. Liu, J. He, G. Zhang, L. M. Peng, Z. Zhang, *ACS Nano* **2020**, *14*, 8866.
[31] R. Campos, J. Borme, J. R. Guerreiro, G. Machado, M. F. Cerqueira, D. Y. Petrovykh, P. Alpuim, *ACS Sens.* **2019**, *4*, 286.
[32] A. Ganguli, Y. Watanabe, M. T. Hwang, J. C. Huang, R. Bashir, *Biomed. Microdevices* **2018**, *20*, 45.
[33] A. Panahi, M. Ghafar-Zadeh, A. Scime, S. Magierowski, E. Ghafar-Zadeh, *IEEE Trans. Instrum. Meas.* **2022**, *71*.
[34] M. Selvaraj, P. Greco, M. Sensi, G. D. Saygin, N. Bellassai, R. D'Agata, G. Spoto, F. Biscarini, *Biosens. Bioelectron.* **2021**, *182*, 113144.
[35] S. Balderston, J. J. Taulbee, E. Celaya, K. Fung, A. Jiao, K. Smith, R. Hajian, G. Gasiunas, S. Kutanovas, D. Kim, J. Parkinson, K. Dickerson, J. Ripoll, R. Peytavi, H. Lu, F. Barron, B. R. Goldsmith, P. G. Collins, I. M. Conboy, V. Siksnys, K. Aran, *Nat. Biomed. Eng.* **2021**, *5*, 713.
[36] K. M. Cheung, J. M. Abendroth, N. Nakatsuka, B. Zhu, Y. Yang, A. M. Andrews, P. S. Weiss, *Nano Lett.* **2020**, *20*, 5982.
[37] J. Kim, S. Y. Park, S. Kim, D. H. Lee, J. H. Kim, J. M. Kim, H. Kang, J. S. Han, J. W. Park, H. Lee, S. H. Choi, *Sci. Rep.* **2016**, *6*, 31984.
[38] L. Kergoat, L. Herlogsson, D. Braga, B. Piro, M. C. Pham, X. Crispin, M. Berggren, G. Horowitz, *Adv. Mater.* **2010**, *22*, 2565.
[39] T. P. Nguy, V. Kilinc, R. Hayakawa, C. Henry-de-Villeneuve, J. M. Raimundo, Y. Wakayama, A. Charrier, *Sens. Actuator. B Chem.* **2022**, *351*, 130956.
[40] Y. Guo, Y. Han, Z. Su, *J. Phys. Chem. B* **2013**, *117*, 14842.
[41] Z. Zhang, J. Liu, *ACS Appl. Mater. Interfaces* **2016**, *8*, 6371.
[42] Y. J. Liao, Y. C. Shiang, C. C. Huang, H. T. Chang, *Langmuir* **2012**, *28*, 8944.

[43] J. J. Hill, C. A. Royer, *Met. Enzymol.* **1997**, *278*, 390.
[44] M. Riede, B. Lüssem, K. Leo, in *Comprehensive Semiconductor Science and Technology*, Elsevier, Amsterdam, Netherlands **2011**, *4*.13, 465.
[45] S. Bontapalle, A. Opitz, R. Schlesinger, S. R. Marder, S. Varughese, N. Koch, *Adv. Mater. Interfaces* **2020**, *7*, 2000291.
[46] E. A. Josephs, T. Ye, *Nano Lett.* **2012**, *12*, 5255.
[47] U. Rant, K. Arinaga, S. Fujita, N. Yokoyama, G. Abstreiter, M. Tornow, *Org. Biomol. Chem.* **2006**, *4*, 3448.
[48] M. Berto, C. Diacci, R. D'Agata, M. Pinti, E. Bianchini, M. Di Lauro, S. Casalini, A. Cossarizza, M. Berggren, D. Simon, G. Spoto, F. Biscarini, C. A. Bortolotti, *Adv. Biosyst.* **2018**, *2*, 1700072.
[49] U. Zschieschang, R. T. Weitz, K. Kern, H. Klauk, *Appl. Phys. A Mater. Sci. Process.* **2009**, *95*, 139.
[50] K. Chennit, N. Delavari, S. Mekhmoukhen, R. Boukraa, L. Fillaud, S. Zrig, N. Battaglini, B. Piro, V. Noël, I. Zozoulenko, G. Mattana, *Adv. Mater. Technol.* **2022**, 2200300.
[51] I. Sarangadharan, A. K. Pulikkathodi, C. Chu, Y. Chen, A. Regmi, P. Chen, C. Hsu, Y. Wang, *ECS J. Solid State Sci. Technol.* **2018**, *7*, 3032.
[52] S. E. Doris, A. Pierre, R. A. Street, *Adv. Mater.* **2018**, *30*, 1706757.
[53] M. Inouye, R. Ikeda, M. Takase, T. Tsuri, J. Chiba, *Proc. Natl. Acad. Sci. USA* **2005**, *102*, 11606.
[54] B. Y. Michel, D. Dziuba, R. Benhida, A. P. Demchenko, A. Burger, *Front. Chem.* **2020**, *8*, 12.